ADDENDUM MODIFYING OF CYCLOID DRIVES WITH TWO-TOOTH DIFFERENCE ON THE EPICYCLOIDAL PLANET GEAR

Ta-Shi Lai [1] and Jia-Ming Lyu [2]
Department of Vehicle Engineering, National Formosa University
Huwei, Yuenlin 63208, Taiwan
[1]Associate professor, [2]Graduate student
Fax: 886(5) 632-1571, e-mail: tslai@ sunws.nfu.edu.tw

Received September 2005, Accepted April 2006
No. 05-CSME-54, E.I.C. Accession 2906

ABSTRACT

This work presents a curve-fitting approach and addendum-modifying procedures to eliminate the cusps of the epicycloidal planet gear for cycloid drives with two-tooth difference. Envelope theory and kinematic gearing can obtain the epicycloidal profiles. Its inevitable cusps are replaced by the smooth Bezier curves. The curve-fitting results indicate that the best curve fitting for Bezier curves is when the control points pass through the cusp of the epicycloidal profiles. For the interpolation of Bezier curves, it is better for the two reference points to be closer. If the curve-fitting curves require tangent continuity, we should apply the interpolation of Bezier curves. Two examples including six cases demonstrate the usefulness of the proposed approach.

Keywords: Curve fitting, Bezier curves, addendum modifying, cycloid drives.

ADDENDUM MODIFIANT L'ENGRENAGE CYCLOÏDAL AVEC UNE DIFFÉRENCE DE DEUX DENTS SUR LA ROUE PLANÉTAIRE ÉPICYCLOÏDALE

RÉSUMÉ

Ce travail présente une approche d'ajustement de courbes et un addendum modifiant des procédures afin d'éliminer les courbes d'une roue planétaire épicycloïdale pour l'engrenage cycloïdal avec une différence de deux dents. Il est possible d'obtenir les profils épicycloïdaux au moyen de la théorie de l'enveloppe et de l'engrenage cinématique. Ses courbes inévitables sont remplacées par des courbes de Bezier lisses. Les résultats de l'ajustement de courbes indiquent que le meilleur ajustement pour les courbes de Bezier se produit lorsque les points de contrôle passent par la courbe des profils épicycloïdaux. Pour l'interpolation des courbes de Bezier, il est préférable que les deux points de référence soient rapprochés. Si les courbes d'ajustement nécessite une continuité tangente, il faut appliquer l'interpolation des courbes de Bezier. Deux exemples, y compris six cas, démontrent l'utilité de l'approche proposée.

Mots clés : ajustement de courbes, courbes de Bezier, addendum modifiant, engrenage cycloïdal.

1. INTRODUCTION

Speed reducers are used widely in various applications for speed and torque conversion. The cycloid drive type is more compact, and provides both higher speed reduction and higher mechanical advantage than planetary gear trains in a single stage [1]. Above all, it has high precision pointing, so that it is an attractive candidate for many current applications. Therefore, Litvin and Feng [2] used differential geometry to generate the conjugate surfaces of cycloidal gearing for one-tooth difference. Since the cycloid drive with two-tooth difference is suitable for the devices with low gear ratios, Chang and Liu [3] researched the cycloid drives with two-tooth difference on under cutting. Lyu and Lai [4] studied the geometric design of the cycloid drives with conical meshing elements for two-tooth difference. The epicycloidal planet profile has cusps on the addendum, whose cusps are an inevitable drawback. With gearing contact, the cusps will cause noise and damage to the gearing elements [5]. Here we present the procedures and mathematical algorithm to eliminate the cusps for improving the performance.

The principle of conjugate surfaces and envelope theory are of major concern in designing the gears and generating the conjugate meshing elements. Litvin [6] researched the meshing of spatial gears and the generation of conjugate surfaces. Tsai and Chin [7] studied the surface geometry of straight and spiral bevel gears. Hanson and Churchill [8] applied the envelope theory to provide new cam design equation. Colbourne [9] proposed a geometry method to find the envelopes of trochoids that applies rotary pumps. Yan and Lai [10] studied the geometric design of a novel elementary planetary gear train with cylindrical tooth-profiles by envelope theory. Pollitt [11] studied some applications of the cycloid machine design. The curve fitting of Bezier curves was initially applied in industry about 1962. Bezier [12] presented the curve fitting for solving the styling design of the cars. Yan and Chen [13] used Bezier curves so that the output motion could pass through a design trajectory for variable input speed servo-controlled slider-crank mechanisms.

This paper presents the procedures and mathematical algorithm on addendum modifying for cycloid drives with two-tooth difference. The coordinate transformation, envelope theory, and fundamental gearing kinematics are applied to obtain the epicycloidal planet gear of the one-tooth and two-tooth difference. Then, Bezier curves are used to eliminate the cusps of epicycloidal profiles. Finally, design examples are presented and CAD is used to construct the 2-D drawing and solid modeling to demonstrate the feasibility of this approach.

2. GEOMETRIC DESIGN

2.1 Coordinate Systems and Coordinate Transformation

Figure 1 (a) shows the topological structure of the conventional cycloid drives. This speed reducer consists of five main members. Member 1 is a frame; member 2 is a ring gear, whose members include the ring gear body (2a), cylindrical meshing elements (2b), and ring gear pins (2c); member 3 is an epicycloidal planet gear; member 4 is a crank; and member 5 is an output disk, whose disk pin is a floating connection with member 3 and member 5a (disk plate). Figure 1(b) shows the main dimensions of the ring gear and epicycloidal planet gear.

In order to analysis the kinematic relationships among these members, coordinate systems corresponding to the cycloid drive should be defined. According to the topological structure of the Fig. 1, we define two fixed and three movable coordinate systems, as shown in Fig. 2. Here the fixed coordinate system $(xyz)_f$ is rigidly connected to the frame, while the fixed coordinate system $(xyz)_b$ is also connected to the frame. Moving coordinate systems $(xyz)_2$, $(xyz)_r$, and $(xyz)_3$ are rigidly connected to the ring gear, the cylindrical meshing element, and the epicycloidal planet gear, respectively. The ring gear rotates about the z_2 axis and the epicycloidal planet gear rotates about the z_3 axis.

Origins o_f and o_2 are coincident and located at the centre of the ring gear, while origins o_b and o_3 are coincident and located at the centre of the epicycloidal planet gear. Origin o_r is coincident and located at the centre of the cylindrical meshing element. Axis x_f is parallel with axis x_b. The directions of axes z_f, z_b, z_2, z_3, and z_r are perpendicular to the xy plane. Angles ϕ_2 and ϕ_3 are the angular displacements of the ring gear and epicycloidal planet gear, respectively. Positive ϕ_2 and ϕ_3 are measured counterclockwise with respect to axis z_2 and axis z_3, respectively. The distance between the centres of the ring gear and the meshing element denoted as d. The distance between the axes of rotation of the ring gear and the epicycloidal planet gear is e. Symbols R_2 and R_3 are the radii of the centrodes of the ring gear and epicycloidal planet gear, respectively.

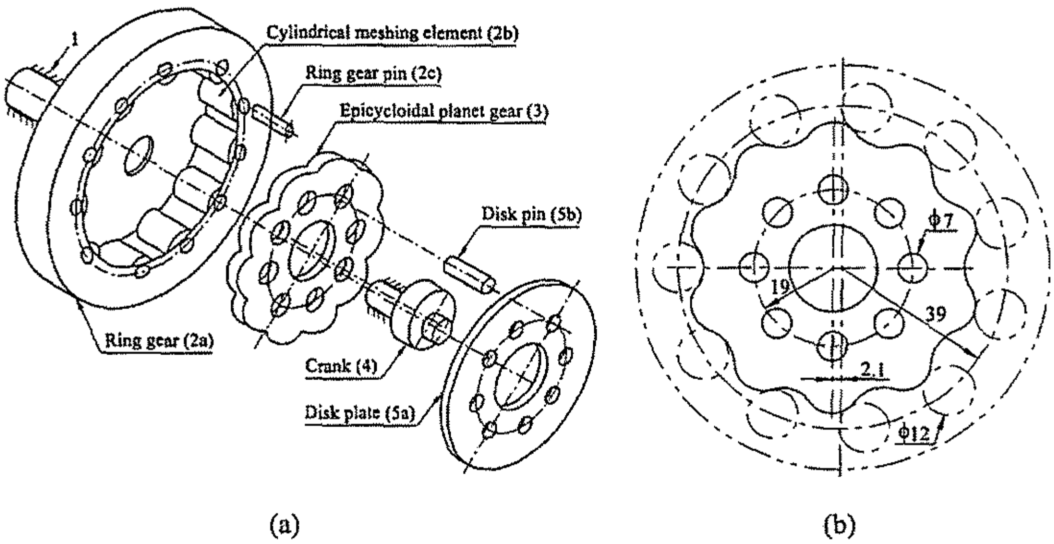

Fig. 1 Topological structure

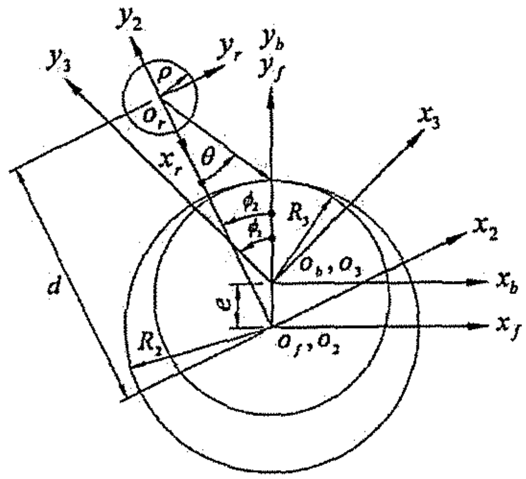

Fig. 2 Coordinate systems

According to the definition of all parameters and coordinate systems, we have the following transformation matrices of the coordinate systems by applying homogeneous coordinates and 4×4 matrices for coordinate transformation [14]. By transforming the coordinate systems from $(xyz)_r$ to $(xyz)_3$, the transformation matrix can be expressed as:

$$[M_{3,r}] = [M_{3,b}][M_{b,f}][M_{f,2}][M_{2,r}]$$
$$= \begin{bmatrix} \cos(\phi_2 - \phi_3) & -\sin(\phi_2 - \phi_3) & 0 & -d\sin(\phi_2 - \phi_3) - (R_2 - R_3)\sin\phi_3 \\ \sin(\phi_2 - \phi_3) & \cos(\phi_2 - \phi_3) & 0 & d\cos(\phi_2 - \phi_3) - (R_2 - R_3)\cos\phi_3 \\ 0 & 0 & 1 & 0 \\ 0 & 0 & 0 & 1 \end{bmatrix} \quad (1)$$

Here, matrix $[M_{3,r}]$ represents the transformation matrix from system r to system 3.

The coordinate system of the cylindrical meshing element is shown in Fig. 3. The coordinate system $(xyz)_r$ is attached to the cylindrical meshing element. The height of the cylindrical meshing element of the ring gear is t. The symbol ρ denotes the radius of the cylindrical meshing element. In coordinate system $(xyz)_r$, the homogeneous coordinates position vector of the cylindrical meshing element can be expressed as:

$$\mathbf{R}_r = [\rho\cos\theta \quad \rho\sin\theta \quad u \quad 1]^T \quad (2)$$

where $0 \le \theta \le 2\pi$, $0 \le u \le t$, and $\mathbf{R}_r$ denotes the surface equation in coordinate system r. Superscript "T" means transposition.

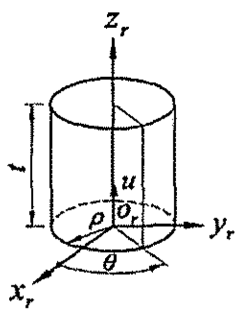

Fig. 3 Cylindrical meshing element

By transforming the equation of the cylindrical meshing element coordinate systems from $(xyz)_r$ to $(xyz)_3$, the surface equation of the cylindrical meshing element can be expressed as:

$$\mathbf{R}_3^r = \left[M_{3,2}\right]\mathbf{R}_2^r = \begin{bmatrix} \rho\sin\theta\cos(\phi_2-\phi_3)-(d-\rho\cos\theta)\sin(\phi_2-\phi_3)-(R_2-R_3)\sin\phi_3 \\ \rho\sin\theta\sin(\phi_2-\phi_3)+(d-\rho\cos\theta)\cos(\phi_2-\phi_3)-(R_2-R_3)\cos\phi_3 \\ u \\ 1 \end{bmatrix} \tag{3}$$

where $\mathbf{R}_3^r$ denotes the r surface equation in coordinate system 3. Let gear ratio $m_{32} = \omega_3 / \omega_2$, then Equation (3) becomes:

$$\mathbf{R}_3^r = \begin{bmatrix} \rho\sin\theta\cos(1-m_{32})\phi_2-(d-\rho\cos\theta)\sin(1-m_{32})\phi_2-(R_2-R_3)\sin m_{32}\phi_2 \\ \rho\sin\theta\sin(1-m_{32})\phi_2+(d-\rho\cos\theta)\cos(1-m_{32})\phi_2-(R_2-R_3)\cos m_{32}\phi_2 \\ u \\ 1 \end{bmatrix} \tag{4}$$

where θ and u are parameters on the particular surface of the family.

2.2 Equation of Meshing and Constrained Conditions

Consider coordinate systems $(xyz)_2$, $(xyz)_r$, $(xyz)_3$, and $(xyz)_f$ that are connected to the ring gear, the cylindrical meshing element, the epicycloidal planet gear, and the frame, respectively. The cylindrical meshing element is provided with a regular surface, Σ_r, that is represented in coordinate system $(xyz)_3$ as follows:

$$\mathbf{R}_r(u,\theta) \in C^1, \quad \frac{\partial \mathbf{R}_r}{\partial u} \times \frac{\partial \mathbf{R}_r}{\partial \theta} \neq \mathbf{0} \tag{5}$$

The symbol C^1 in Equation (5) indicates that the functions $x(u,\theta)$ and $y(u,\theta)$ have continuous derivatives to the first order, at least. From the necessary conditions of existence of surfaces [15], the equation of meshing can be obtained as follows:

$$\left(\frac{\partial \mathbf{R}_3^r}{\partial u} \times \frac{\partial \mathbf{R}_3^r}{\partial \theta}\right) \cdot \frac{\partial \mathbf{R}_3^r}{\partial \phi_2} = 0 \tag{6}$$

Equation (6) relates the curvilinear coordinates (u,θ) of surface Σ_r with the generalized parameter of motion, ϕ_2. By differentiating Equation (4) with respect to the u, θ, and ϕ_2, respectively, then substituting them into Equation (6), we can obtain the equation of meshing as follows:

$$\tan\theta = \frac{\sin\phi_2}{(d/R_2)-\cos\phi_2} \tag{7}$$

Figure 4 shows the geometrical relationships between the cylindrical meshing elements. In order to avoid interference between the near cylindrical meshing elements, the meshing element radius must be constrained in the following inequality.

$$\rho < d\sin(\frac{\pi}{N_2}) \tag{8}$$

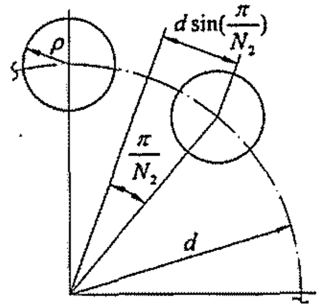

Fig. 4 Geometrical relationships of cylindrical meshing elements

Simultaneously solving Equations (4) and (7)-(8), the epicycloidal profiles can be obtained for cycloid drives with one-tooth difference. From the kinematic gearing theory, for cycloid drives with tooth-difference, that the relationships of the parameters R_2, R_3, e, N_2, N_3, and p_c can be expressed as follows [16]:

$$2\pi R_2 = 2\pi R_3 + (N_2 - N_3)p_c \tag{9}$$

$$R_2 = \frac{N_2 e}{N_2 - N_3} \tag{10}$$

$$R_3 = \frac{N_3 e}{N_2 - N_3} \tag{11}$$

where N_2 and N_3 are the number of the cylindrical meshing elements and epicycloidal planet gear teeth (or lobes), respectively. Symbol p_c denotes the circular pitch. By combining Equations (4) and (7)-(11), epicycloidal profiles can be obtained for cycloid drives with two-tooth difference.

2.3 Flowchart and Numerical Examples

Figure 5 shows the flow chart of the design and addendum modifying for cycloid drives. When the major parameters of the cycloid drive are given as shown in table 1, we may obtain the epicycloidal profiles for one-tooth and two-tooth difference. Figures 6(a) and (b) show the epicycloidal profiles and cylindrical meshing elements for one-tooth and two-tooth difference, respectively.

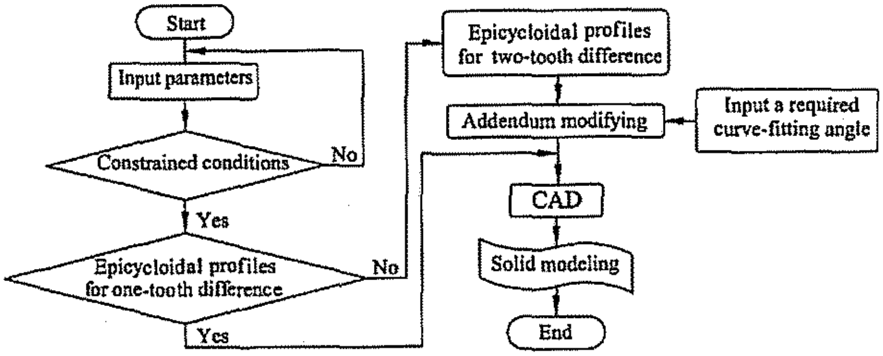

Fig. 5 Flow chart of the design and addendum modifying for cycloid drives

Table 1 Design parameters of the cycloid drives

Parameters	d	e	ρ	N_2	N_3	R_2	R_3	t
For one-tooth difference	90	4	7	11	10	44	40	10
For two-tooth difference	90	4	7	22	20	44	40	10
Unit	mm	mm	mm			mm	mm	mm

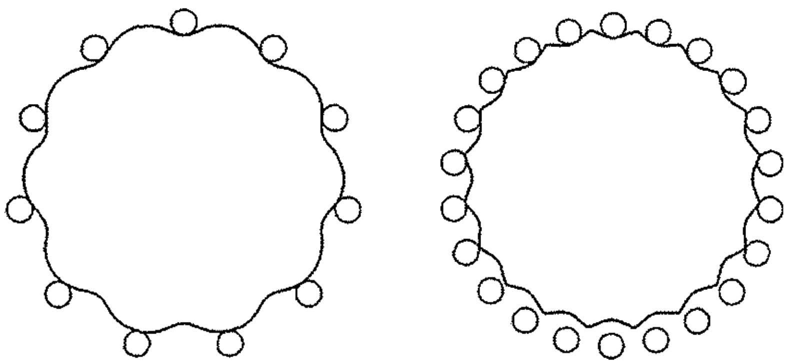

(a) One-tooth difference (b) Two-tooth difference

Fig. 6 Epicycloidal profiles and cylindrical meshing elements

Using above geometric design results, we apply CAD (Pro/ENGINEER) to construct the solid modeling of the epicycloidal planet gear, as shown in Fig. 7.

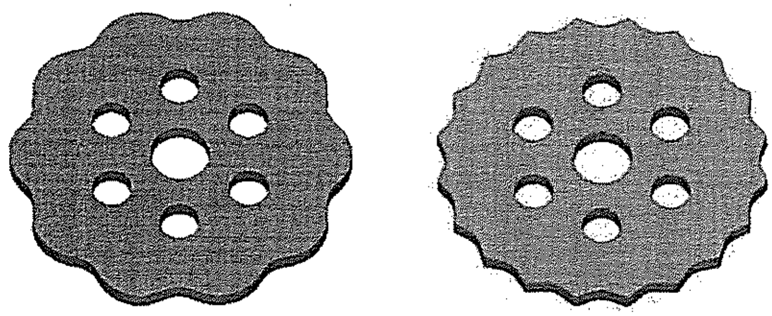

(a) One-tooth difference (b) Two-tooth difference

Fig. 7 Solid modeling of the epicycloidal planet gear

3. CURVE FITTING AND ADDENDUM MODIFYING

There are inevitable cusps on the epicycloidal planet gear of the cycloid drives with two-tooth difference, which will reduce the performance and available life. Therefore, it is very important to eliminate the cusps in designing and manufacturing. Here we use Bezier curves to replace the local original epicycloidal profiles.

We hereby introduce the Bezier curves to present the curve fitting on the addendum of the epicycloidal profiles, as proposed in the early 1960s for the design of car styling. Bezier curves have the advantages that we can change arbitrary control points to modify the curve shape and predict the curve region.

A Bezier curve is a curve whose shape is defined by a set of control points. The order of a Bezier curve is related to the number of control points defining it; $n+1$ points define an nth order curve. Bezier curves and surfaces are credited to $\mathbf{P}(w)$. Mathematically, a Bezier curve $\mathbf{P}(w)$ is defined by the following polynomial as:

$$\mathbf{P}(w)=\sum_{i=0}^{n}\mathbf{P}_i \times \mathrm{B}_{i,n}(w) \qquad w\in[0,1] \tag{12a}$$

$$\mathrm{B}_{i,n}(w)=(\frac{i}{n})\times w^i \times (1-w)^{n-i} \tag{12b}$$

$$(\frac{i}{n})=\frac{n!}{i!(n-i)!} \tag{12c}$$

If the Bezier curve is a third order curve, then Equation (12) can be expressed as following scalar equations:

$$P_x(w)=(1-w)^3 x_0 + 3w(1-w)^2 x_1 + 3w^2(1-w)x_2 + w^3 x_3 \tag{13a}$$

$$P_y(w)=(1-w)^3 y_0 + 3w(1-w)^2 y_1 + 3w^2(1-w)y_2 + w^3 y_3 \tag{13b}$$

$$P_z(w)=(1-w)^3 z_0 + 3w(1-w)^2 z_1 + 3w^2(1-w)z_2 + w^3 z_3 \tag{13c}$$

Where P_x, P_y, and P_z are the components of the coordinate system in the x, y, and z directions, respectively. The shape of the Bezier curve $\mathbf{P}(w)$ is controlled by a set of P_i. From Equation (13) we can obtained a third Bezier curve as shown in Fig. 8. The curve starts at P_0 where $w=0$, and ends at P_3 where $w=1$. The shape of the curve where $0 \le w \le 1$ can be arbitrary adjusted by the positions of the control points P_1 and P_2.

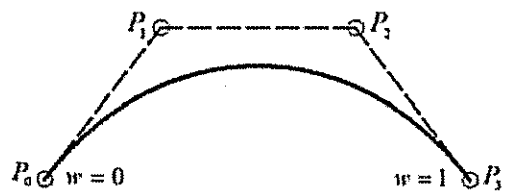

Fig. 8 Third order Bezier curve

The dashed line in Fig. 8 is the characteristic polygon for Bezier curves.

If we desire the curve-fitting curve of Bezier curves with the tangent continuity behavior, then the curve fitting of the interpolation of Bezier curves should be considered. Figure 9 shows the interpolation of Bezier curves for a third order. Assuming q_0, q_1, q_2, and q_3 are given reference points, then their control points P_0', P_1', P_2', and P_3' can be obtained as follows:

$$\overline{T_1} = w_1 L \hat{t}_1 \tag{14a}$$

$$\overline{T_2} = w_2 L \hat{t}_2 \tag{14b}$$

$$\hat{t}_1 = \frac{q_1 - q_0}{|q_1 - q_0|} \tag{14c}$$

$$\hat{t}_2 = \frac{q_3 - q_2}{|q_3 - q_2|} \tag{14d}$$

$$L_1 = |q_1 - q_0|, \quad L_2 = |q_2 - q_3| \tag{14e}$$

where $L = |q_2 - q_1|$, $w_1 = L_2/(L_1 + L_2)$, and $w_2 = L_1/(L_1 + L_2)$.

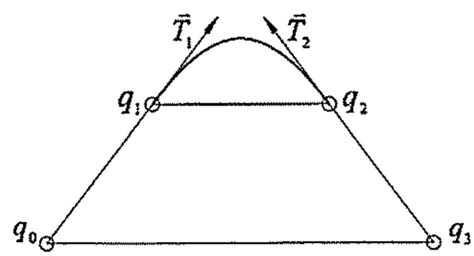

Fig. 9 Third order for the interpolation of Bezier curve

From Equation (14) we can express the curve fitting of the interpolation of Bezier curves for a third order as follows:

$$\mathbf{P}'(w)=(1-w)^3\mathbf{P}_0'+3w(1-w)^2\mathbf{P}_1'+3w^2(1-w)\mathbf{P}_2'+w^3\mathbf{P}_3' \qquad w\in[0,1] \tag{15}$$

where $P_0'=q_1$, $P_3'=q_2$, $P_1'=q_1+T_1$, and $P_2'=q_2-T_2$. Equation (15) can be expressed as the following scalar equations:

$$P_x'(w)=(1-w)^3x_0+3w(1-w)^2x_1+3w^2(1-w)x_2+w^3x_3 \tag{16a}$$

$$P_y'(w)=(1-w)^3y_0+3w(1-w)^2y_1+3w^2(1-w)y_2+w^3y_3 \tag{16b}$$

$$P_z'(w)=(1-w)^3z_0+3w(1-w)^2z_1+3w^2(1-w)z_2+w^3z_3 \tag{16c}$$

The epicycloidal profiles are periodic, so we can use a single tooth profile to make curve fitting. The rest of tooth profiles can be obtained by the following equations:

$$r_i^2=x_i^2+y_i^2 \tag{17}$$

$$\theta_i=\arctan\frac{y_i}{x_i} \tag{18}$$

$$x_j=r_i\cos(\theta_i+\delta) \tag{19}$$

$$y_j=r_i\sin(\theta_i+\delta) \tag{20}$$

$$\delta=2k\pi/N_3 \qquad k=1,2,3.......(N_3-1) \tag{21}$$

Example 1. We use three cases to make the curve fitting of Bezier curves for addendum modifying. The control points are shown in table 2.

Table 2 Control points of Bezier curves

Control points	P_0	P_1	P_2	P_3
Case 1	(0, 79)	(8.5183, 81.4492)	(17.0678, 80.0951)	(24.3245, 75.1624)
Case 2	(8.5183, 81.4492)	(11.4629, 82.5944)	(14.6213, 82.0941)	(17.0678, 80.0951)
Case 3	(8.5183, 81.4492)	(13.1627, 83.1061)	(13.1627, 83.1061)	(17.0678, 80.0951)

Substituting the above control points into Eqs. 13(a) and (b), the Bezier curves can be obtained. Figure 10 shows a single tooth profile of the epicycloidal profile and its Bezier curve for case 1, where α denotes the angle between the two end points for a single tooth profile. The specified required curve-fitting angle is α for this case. Let angles $\alpha=2\pi/N_3$ and $\beta=\alpha/3$. The symbol P_i denotes the control points of Bezier curves. The control points P_0 and P_3 are specified at the two end points of the single tooth epicycloidal profile in this case.

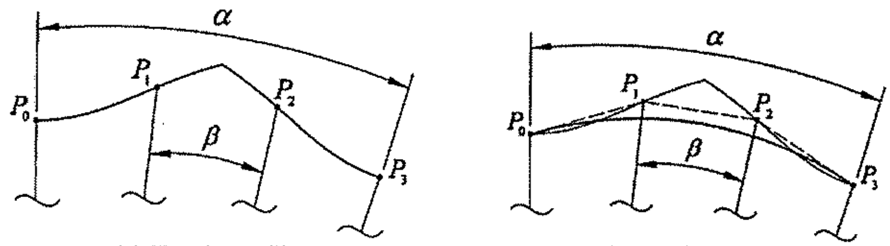

(a) Tooth profile (b) Bezier curve

Fig. 10 Single tooth profile for epicycloidal profiles (example 1, case 1)

Figure 11 illustrates the relationships of the control points for a single tooth profile and the Bezier curve for case 2, specifying the required curve-fitting angle β for this case. The points P_1 and P_2 are chosen within the points P_0 and P_3.

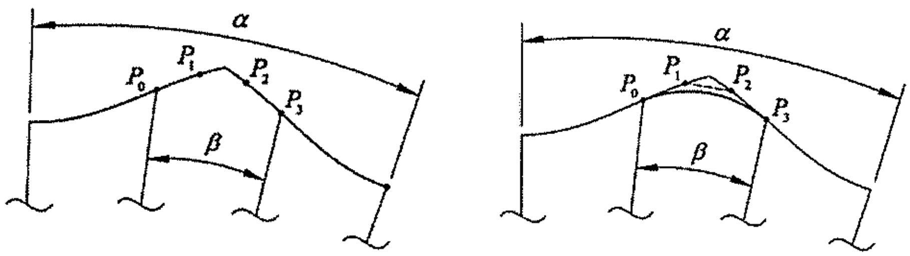

(a) Tooth profile (b) Bezier curve

Fig. 11 Single tooth profile for epicycloidal profiles (example 1, case 2)

Figure 12 shows a single tooth profile of epicycloidal profiles and its Bezier curve for case 3. Specified the required curve-fitting angle is β, while let control points P_1 and P_2 on the cusp of the single tooth epicycloidal profile for this case.

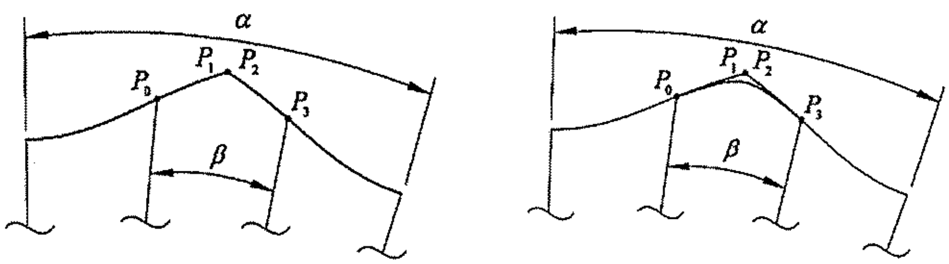

(a) Tooth profile (b) Bezier curve

Fig. 12 Single tooth profile for epicycloidal profiles (example 1, case 3)

Figure 13 shows the results of Bezier curves and the original tooth profile for example 1. The symbols delta, circle, and square denote cases 1, 2, and 3, respectively. Comparing the results, it can be seen that the case 3 is the best curve fitting for the original tooth profile.

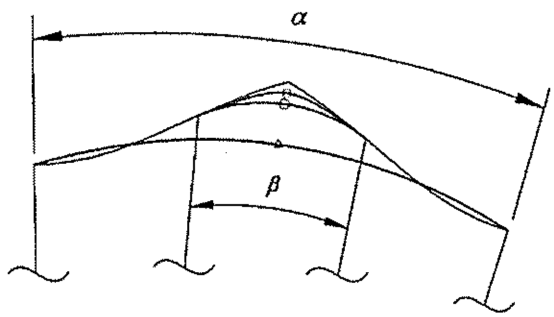

Fig.13 Bezier curves for example 1

Substituting the above results into Equations (17)-(21) we can obtain the epicycloidal planet profiles for example 1, as shown in Figure 14. This illustrates that case 1 is the worst curve fitting of the three cases.

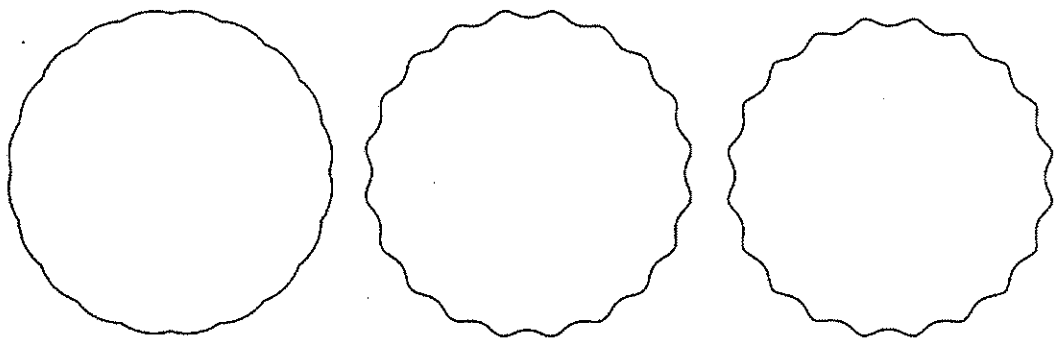

(a) Case 1 (b) Case 2 (c) Case 3

Fig. 14 Epicycloidal profiles after addendum modified for example 1

Example 2. We use three cases to make the curve fitting of the interpolation of Bezier curves for addendum modifying. The reference point q_i and control point $P_i^{'}$ are shown in table 3.

Table 3 Reference and control points for the interpolation of Bezier curves

Examples	Reference and control points			
Case 1	q_0(0, 79) $P_0^{'}$(8.5183, 81.4492)	q_1 (8.5183, 81.4492) $P_1^{'}$(12.6569, 82.6391)	q_2(17.0678, 80.0951) $P_2^{'}$(13.4704, 82.5404)	q_3(24.3245, 75.1624) $P_3^{'}$(17.0678, 80.0951)
Case 2	q_0(5.1893, 80.0418) $P_0^{'}$(8.5183, 81.4492)	q_1(8.5183, 81.4492) $P_1^{'}$(12.5047, 83.1345)	q_2(17.0678, 80.0951) $P_2^{'}$(13.7974, 82.9299)	q_3(19.7989, 77.7278) $P_3^{'}$(17.0678, 80.0951)
Case 3	q_0(8.4610, 81.4246) $P_0^{'}$(8.5183, 81.4492)	q_1(8.5183, 81.4492) $P_1^{'}$(12.4980, 83.1593)	q_2(17.0678, 80.0951) $P_2^{'}$(13.8188, 82.9491)	q_3(17.1147, 80.0539) $P_3^{'}$(17.0678, 80.0951)

Substituting the reference points into Equation (14), and control points into Equations 16(a) and (b), the interpolation of Bezier curves can be obtained. Figure 15 shows a single tooth profile of epicycloidal profile and its interpolation of Bezier curve for case 1. We chose reference points q_0 and q_3 at the two ends of the single tooth epicycloidal profile.

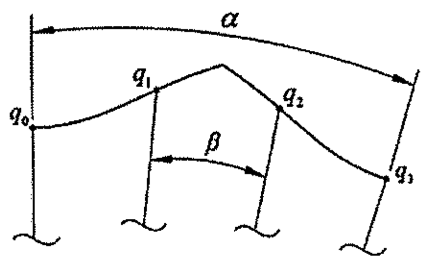

(a) Tooth profile (b) Bezier curve by interpolation

Fig. 15 Single tooth profile for epicycloidal profiles (example 2, case 1)

Figure 16 shows a single tooth profile of epicycloidal profile and its interpolation of Bezier curve for case 2. The point q_0 is far from point q_1.

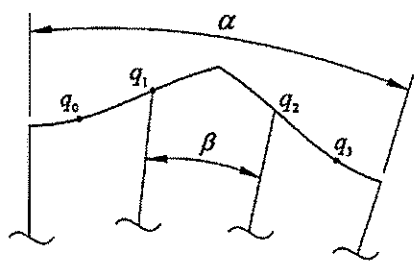

(a) Tooth profile (b) Bezier curve by interpolation

Fig.16 Single tooth profile for epicycloidal profiles (example 2, case 2)

Figure 17 shows a single tooth profile of epicycloidal profile and its interpolation of Bezier curve for case 3. The reference points, q_0 and q_1, are very close in this case.

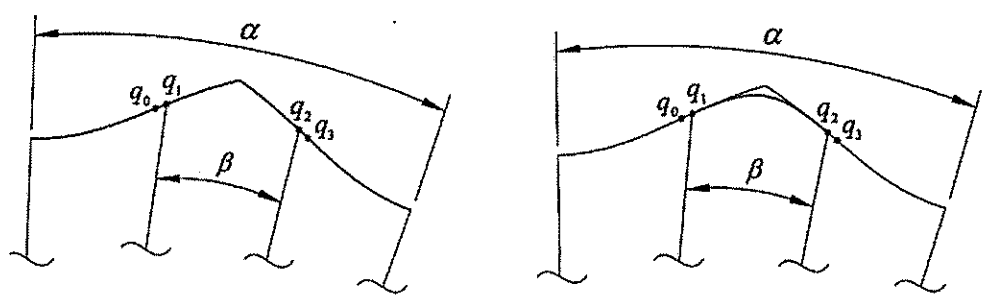

(a) Tooth profile (b) Bezier curve by interpolation

Fig.17 Single tooth profile for epicycloidal profile (example 2, case 3)

Figure 18 shows the results for the interpolation of Bezier curves and the original tooth profile for example 2. The symbols delta, circle, and square denote cases 1, 2, and 3, respectively. The results indicate that the case 3 is the best curve fitting for these cases.

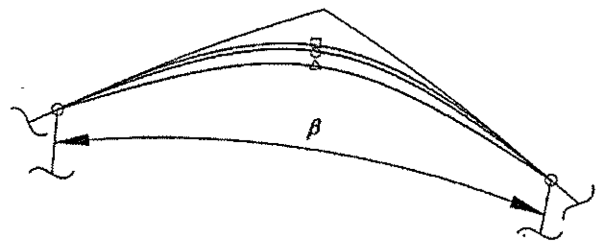

Fig. 18 Interpolation curve fitting of Bezier curves for example 2

Substituting the example 2 results into Equations (17)-(21), we can obtain the epicycloidal profiles after addendum modified, as shown in Fig. 19.

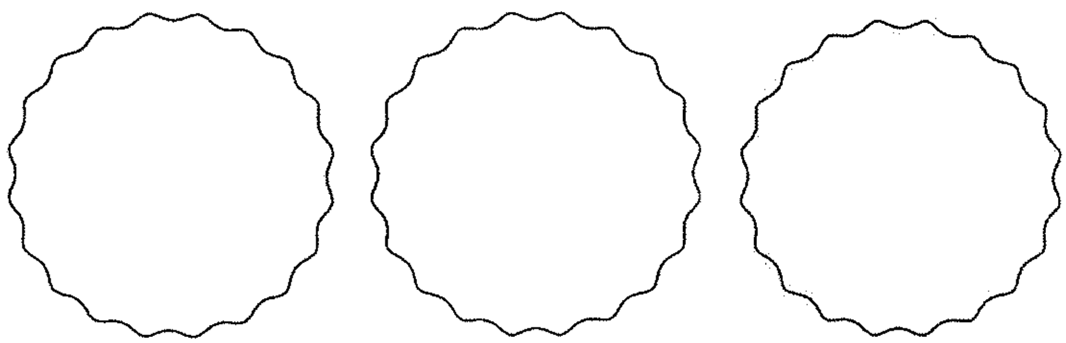

(a) Case 1 (b) Case 2 (c) Case 3

Fig. 19 Epicycloidal profiles after addendum modified for example 2

Figure 20 shows the case 3 results for examples 1 and 2. The dashed line and the solid line are examples 1 and 2, respectively. Comparing the two curves there is almost the same curve-fitting effect, but example 1 can only obtain the position continuity.

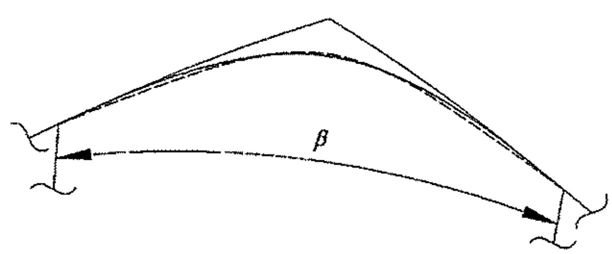

Fig. 20 Epicycloidal profiles for examples 1 and 2

Using the above results, we apply CAD (Pro/ENGINEER) to construct solid modeling, for example 2 (case 3), as shown in Fig. 21.

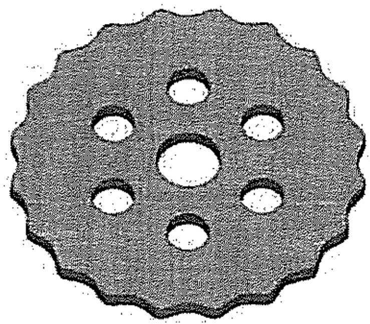

Fig. 21 Solid modeling after addendum modified for example 2 (case3)

4. CONCLUSIONS

This paper applies envelope theory and kinematic gearing to obtain the epicycloidal profiles with one-tooth and two-tooth difference. We further use a curve-fitting approach and addendum-modifying procedures to eliminate the cusps of the epicycloidal planet gear for cycloid drives with two-tooth difference. From the results of the curve fitting of Bezier curves, there is better curve fitting as the control points are closer the cusps of the epicycloidal profiles. As the control points are further from the cusps, the Bezier curve maybe lead to a little interference with meshing elements. The curve fitting for the interpolation of Bezier curves is better as the two reference points are closer. Comparing these two curve-fitting types, the Bezier curve can only have the behavior of the position continuity. Six epicycloidal profiles and one solid modeling are presented to demonstrate that the procedures and approach are feasible.

ACKNOWLEDGMENTS

The authors are grateful to the National Science Council of the Republic of China (Taiwan) for supporting this research under grant NSC94-2212-E-150-015.

REFERENCES

[1] Botsiber, D. W. and Kingston, L., "Design and Performance of the Cycloid Speed Reducer," *Mechanical Design*, June 28, pp. 65-69 (1956).
[2] Litvin, F. L. and Feng, P. H., "Computerize Design and Generation of Cycloidal Gearing," *Mechanism and Machine Theory*, Vol. 31, pp. 891-911, (1996).
[3] Chang, S. L. and Liu, J. Y., "Mathematical model and undercutting analysis of epitrochoid gear for the cycloid drives," International Conference on Gearing, Transmissions and Mechanical Systems, Ed. Daizhong Su, Professional Engineering Publishing, London (U.K.), pp. 293-303 (2000).
[4] Lyu, J.M. and Lai, T.S., Geometric Design of Cycloid Drives with Two Teeth Difference On Conical Tooth Profiles," Proceedings of the Seventh National Conference on the Design of Mechanisms and Machines, The Chinese Society of Mechanism and Machine Theory, pp. 285-290 (2004).
[5] Shu, H., Chiu, H. H., Tsai, C. Y., Wang, K., and Yu, C., Mechanical Design Hand Book, Vol. 3, Chien Hong Publisher, Taipei, Taiwan, pp. 24-121 (1995).
[6] Litvin, F. L., "The Synthesis of Approximate Meshing for Spatial Gears," *Journal of Mechanisms*, Vol. 4, pp. 187-191 (1968).

[7] Tsai, Y. C. and Chin, P. C., "Surface Geometry of Straight and Spiral Bevel Gears, " *ASME Transactions, Journal of Mechanisms, Transmissions, and Automation in Design*, Vol. 109, pp. 443-449 (1987).
[8] Hanson, D. R. S. and Churchill, F. T., "Theory of Envelope Provided New Cam Design Equation," *Product Engineering*, pp. 45-55 (1962).
[9] Colbourne, J. R., "The Geometry of Trochoid Envelopes and Their Application in Rotary Pumps," *Mechanism and Machine Theory*, Vol. 4, pp. 421-435 (1974).
[10] Yan, H. S. and Lai, T. S., "Geometry Design of A Novel Elementary Planetary Gear Trains with Cylindrical Tooth-Profiles," *Journal of the Mechanical and Machine Theory*, vol. 37, pp. 757-767 (2002).
[11] Pollitt, E. P., "Some Applications of the Cycloid Machine Design," ASME Journal of Engineering for Industry, November, pp. 407-414 (1960).
[12] P. E. Bezier, "Example of an Existing Eystem in the Motor industry, The Unsure System." Proc. Roy. Soc. London, Vol. A321, pp. 207-218 (1971).
[13] Hong-Sen Yan and Wei-Ren Chen, "On the output motion characteristics of variable speed input servo-controlled slider-crank mechanisms," Mechanism and Machine Theory, Vol. 35, No. 4, pp. 541-561 (2000).
[14] Denavit, J. and Hartenberg, R. S., "A Kinematic Notation for Lower Pair Mechanisms Base on Matrices," ASME Transactions, Journal of Applied Mechanics, Vol. 22, No. 2, pp. 215-221 (1955).
[15] H. S. M. Coxeter, Introduction to Geometry, University of Toronto, Toronto, (1961).
[16] Litvin, F. L., Gear Geometry and Applied Theory, PTR Prentice Hall, Englewood Cliffs, (1994).

NOMENCLATURE

e	Distance between the centres of ring gear and epicycloidal planet gear
$[M_{3,r}]$	Coordinate transformation matrix from system r to system 3
R_2	Radius of the centrodes of the ring gear
R_3	Radius of the centrodes of the epicycloidal planet gear
t	Height of the tooth of epicycloidal planet gear
N_2	The number of ring-gear meshing elements
N_3	The number of epicycloidal planet gear teeth (lobes)
$\mathbf{R}_i$	Surface equation in coordinate system i
$\mathbf{R}^i_j$	The i surface equation in coordinate j
u, θ	Curvilinear coordinates on the surface of the cylindrical meshing element
$(xyz)_2$	Moving coordinate system rigidly connected to the ring gear
$(xyz)_3$	Moving coordinate system rigidly connected to the epicycloidal planet gear
$(xyz)_b$	Fixed coordinate system rigidly connected to the frame at point b
$(xyz)_f$	Fixed coordinate system rigidly connected to the frame at point f
$(xyz)_r$	Moving coordinate system rigidly connected to the cylindrical meshing element
ϕ_2	Angular displacement of the ring gear
ϕ_3	Angular displacement of the epicycloidal planet gear
Σ_2	Ring gear surface
Σ_r	Cylindrical meshing element surface
ρ	Radius of cylindrical meshing element